Deriving connectivity from spiking activity in detailed models of large-scale cortical microcircuits

Faraz Moghbel[1,2], Muhammad Taaha Hassan[1], Alexandre Guet-McCreight[1], Heng Kang Yao[1,2], and Etay Hay[1,2,3*]

[1] Krembil Centre for Neuroinformatics, Centre for Addiction and Mental Health, Toronto, ON M5T 1R8, Canada
[2] Department of Physiology, University of Toronto, Toronto, ON M5S 1A1, Canada
[3] Department of Psychiatry, University of Toronto, Toronto, ON M5S 1A1, Canada
*Correspondence: etay.hay@camh.ca

Abstract

Inferring detailed cortical microcircuit connectivity is essential for uncovering how information is processed in the brain. A common method *in vivo* uses short-lag spike cross-correlations to derive putative monosynaptic connections, but inactive neurons and correlated firing can hinder the derivation accuracy. Previous computational studies that developed methods to derive connectivity from cross-correlations employed simplified or small network models and thus did not address the above key confounds of physiological large-scale networks. We tested connectivity derivation using simulated ground-truth spiking from detailed models of human cortical microcircuits in different layers and between key neuron types. While derivation accuracy was high for cortical layer 5 microcircuits, we showed that low firing and inactive neurons in layer 2/3 microcircuits resulted in poor performance. We then showed that general activation paradigms for layer 2/3 microcircuits led to only a moderate improvement in derivation performance, due to a trade-off between reducing the proportion of inactive neurons and increasing correlated overactive neurons. We further improved the connection derivation performance using a more refined activation paradigm leading to jittered moderate spiking, which decreased inactive neurons without incurring unwanted correlations. Our results address key physiological challenges and provide methods to improve performance in deriving connections from spiking activity in large-scale neuronal microcircuits.

Introduction

Information processing in the brain is governed by the activity of diverse neuron types[1–3] with specific connectivity[4–7]. Accordingly, cortical dysfunction has been associated with changes in microcircuit connectivity[8–11]. Accurately inferring the underlying cortical microcircuit connectivity is therefore essential for uncovering how information is processed in the brain in health and disease. Short-lag correlations from pairwise extracellular spiking have been commonly used to derive monosynaptic connectivity *in vivo*[12–14], and using these methods with high-density Neuropixels probes[15,16] can enable derivation of larger scale connectivity. However, studies have yet to address key physiological confounds of large-scale derivation such as inactive neurons[17] and correlated network activity[18].

There are several common methods for deriving connections, each with its advantages and limitations. Intracellular paired recordings of postsynaptic potentials (PSP) enable direct detection and measuring of synaptic connection strength[19], but are limited in scale to at most a dozen neurons simultaneously[5]. Recent advancements allow for the switching of the neurons that are being recorded, to yield tens of neurons from a single microcircuit[20]. Conversely, volume electron microscopy[21,22] offers a means for larger-scale connectome reconstruction of segments as large as 1 mm^3 [23–25], but these structural methods are limited in their ability to quantify synaptic connection strength[26,27]. Short lags in spike cross-correlations between pairs of neurons from extracellular recordings[12,13] enable deriving putative monosynaptic connections and strengths[28,29] *in vivo*, and recent high-density Neuropixels probes[15] that record spiking in hundreds of neurons simultaneously[16,30] offer the advantage of estimating connections at large scale.

Physiological confounds need to be considered when deriving connectivity in realistic large-scale networks. Correlated activity of neuronal microcircuits due to oscillations[18] or shared inputs[31,32] can lead to spurious derived connections. Inactive or silent neurons, for which spiking information is lacking, often constitute a significant portion of the neurons in the network, up to 30% in cortical layer 2/3 (L2/3)[17,33–35], and can lead to missed connections. Other physiological properties such as detailed neuron morphologies, multiple synaptic contacts, and stochastic release probabilities, all contribute to a more complex relationship between synaptic inputs and spike output[36], which may impose challenges in connection derivation from cross-correlations.

Previous efforts have taken different approaches to improve neuronal connectivity derivation. Generalized linear models fit to cross-correlograms were used to improve the

derivation performance and to estimate synaptic weights corresponding to PSPs[37,38]. Supervised learning algorithms have been used to infer synaptic weights from presynaptic spike trains of simulated networks[39], and with activation paradigms to address silent neurons[40]. Other studies developed methods to derive network connectivity from multiple samples via statistical connectivity inferencing[41,42]. However, all these previous studies used simplified small network models that did not address challenges of large-scale physiological microcircuits such as silent neurons and correlated activity due to circuit dynamics.

Here we test methods for deriving connections from cross-correlations using simulated ground-truth spiking data from recent detailed large-scale models of human cortical microcircuits[43,44], accounting for several key physiological challenges. We characterize the derivation performance for microcircuits in different cortical layers, and test general and refined activation paradigms to improve connection derivation. In addition to excitatory connections, we also examine derivation for inhibitory connection of different cell types in the cortical microcircuits.

Results

We examined the derivation of putative monosynaptic connections from spike cross-correlations during baseline activity in cortical microcircuits with moderate vs low firing rates. We used simulated ground-truth data from our previous detailed models of human cortical layer 5 (L5) and L2/3 microcircuits, which have moderate and low baseline firing rates of pyramidal (Pyr) neurons, respectively (3.3 ± 1.0 Hz vs 0.8 ± 0.6 Hz, Cohen's $d = 2.96$, $p < 0.05$, Figure 1A-B). We used recent tools of fitting generalized linear models to cross-correlograms, featuring a slow fluctuation curve to absorb correlation trends in baseline activity over longer time courses[37,38] (Figure 1C).

Deriving excitatory connections across the moderately active L5 Pyr neurons (n = 700) had good performance accuracy (sensitivity = 88.2 ± 7.5%, positive predictive value (PPV) = 84.5 ± 6.6%, specificity = 98.3 ± 0.9%, Figure 1D). The L5 Pyr neuron baseline activity involved sufficient spiking for detecting pairwise short-lag correlations, where the slow fluctuation curve fit the long-lag dynamics well using a flatness parameter (γ) of 2×10^{-4} ms^{-1}, and short-lag peaks were fit well when testing for connections in a 4 – 8 ms window (Figure 1C). In contrast, the lack of spikes in low firing L2/3 Pyr neurons made it more difficult to detect short-lag peaks compared to baseline activity (Figure 1C), resulting in poor connection derivation performance (sensitivity = 5.6 ± 6.3%, n = 784 postsynaptic neurons, Figure 1D).

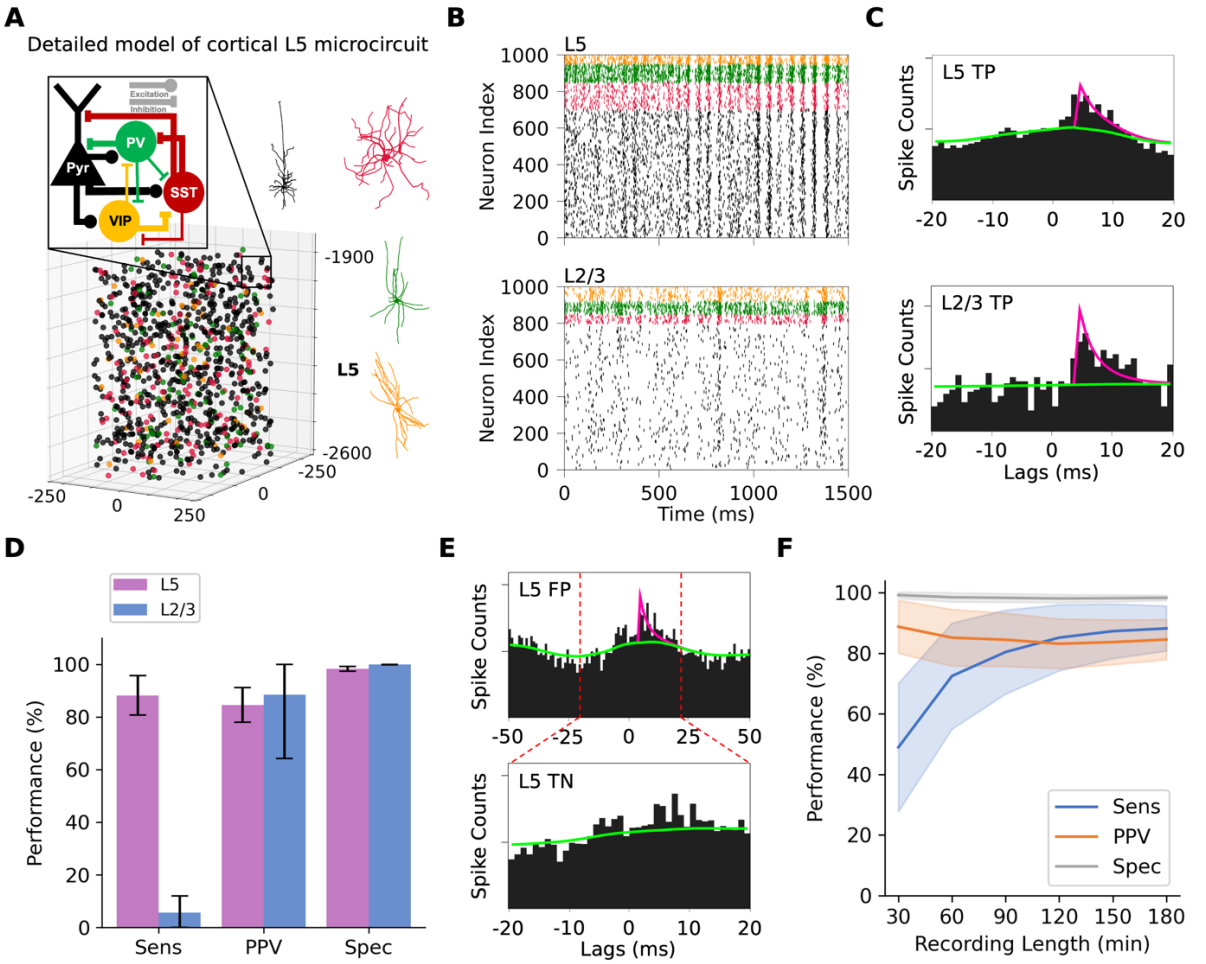

Figure 1. Characterizing physiological confounds when deriving excitatory connections in L5 and L2/3 microcircuits. (A) Top: The detailed model of a human cortical L5 microcircuit comprised of 1,000 neurons of the key types (Pyr neurons, somatostatin-expressing (SST) interneurons, parvalbumin-expressing (PV) interneurons, and vasoactive intestinal peptide-expressing (VIP) interneurons) with detailed morphologies, distributed in a 500 x 500 x 700 μm^3 volume. Inset: schematic diagram of the excitatory and inhibitory connections between neuron types. **(B)** Example raster plots of baseline neuronal spiking in L5 (top) and in L2/3 (bottom) used for connection derivation, color-coded according to neuron type. **(C)** Cross-correlogram, derived connection (magenta) and slow fluctuation curve (green) for example true positive derived excitatory connections in the L5 (top) and L2/3 (bottom) microcircuits. **(D)** Derivation performance for L5 (purple, n = 700 postsynaptic Pyr neurons) and L2/3 (blue, n = 784 postsynaptic Pyr neurons) excitatory connections using a ± 20 ms cross-correlation lag analysis window. **(E)** Example false positive L5 excitatory connection derivation at ± 50 ms window (top), which was correctly identified as a true negative using the ± 20 ms window (bottom). **(F)** Derivation performance as a function of the length of simulated spike data in L5, using the ± 20 ms window. Plots in D and F show mean ± SD.

We used a ± 20 ms cross-correlation lag analysis window, as it improved connection derivation by shortening the analysis window relative to the oscillation period. Using longer cross-correlogram windows such as ± 50 ms or ± 200 ms, as in previous works[37], led to worse sensitivity and PPV (sensitivity = 83.0 ± 5.7%, Cohen's d = -0.79, $p < 0.05$; PPV: 67.3 ± 6.8%, Cohen's d = -2.57, $p < 0.05$, Figure 1E). While the slow fluctuation curve helped derivation, it could not sufficiently mitigate the effects of highly correlated activity, seen especially in the

longer windows (Figure 1E), regardless of the parameter values. For example, even using a wave period that closely fit the long-lag dynamics in the analysis window did not improve the derivation, as it increased the proportion of false negatives. Excluding connections that peaked around lag 0 (between -1 and 1 ms, indicating correlated activity rather than necessarily a connection) did not improve derivation either, as it improved PPV (85.3 ± 6.8%, Cohen's d = 2.66, $p < 0.05$) at the cost of reduced sensitivity (73.8 ± 9.0%, Cohen's d = -1.22, $p < 0.05$).

There was a steady improvement in derivation performance with the length of simulated data up to 120 minutes (30 min vs 120 min: sensitivity = 49.0 ± 21.2% vs 85.2 ± 10.9%, Cohen's d = 2.15, $p < 0.05$, Figure 1F), beyond which the improvement was only marginal (120 min vs 180 min: sensitivity = 85.2 ± 10.9% vs 88.2 ± 7.5%, Cohen's d = 0.32, $p < 0.05$, Figure 1F).

We therefore tested a general activation of L2/3 Pyr neurons by increasing their background input (hereafter referred to as L2/3 general-Pyr), thus increasing the mean firing rate to 3.3 ± 2.4 Hz, close to that in L5 (Figure 2A). Derivation performance for the L2/3 general-Pyr paradigm had higher sensitivity (52.7 ± 14.0%, Cohen's d = 4.34, $p < 0.05$, n = 786 neurons, Figure 2B), although still low compared to the derivation from the L5 microcircuit. While the general-Pyr activation decreased PPV to some extent (L2/3 baseline: PPV = 88.4 ± 24.2%, n = 784 neurons; L2/3 general-Pyr: PPV = 69.9 ± 13.7%, Cohen's d = -0.94, $p < 0.05$, n = 786 neurons, Figure 2B), the increase in sensitivity was much larger, therefore the derivation performance was overall better and more balanced than at baseline.

A likely reason for the moderate improvement in L2/3 general-Pyr was indicated by the distribution of average Pyr neuron spike rates (Figure 2A). While the Pyr neurons in L2/3 general-Pyr had much less inactive neurons compared to baseline L2/3, there were still 17% (n = 133) inactive neurons firing at < 1 Hz, and the sensitivity in deriving connections for these neurons was poorer than average (12.4 ± 10.9%, Cohen's d = -2.97, $p < 0.05$). There was also a larger right tail compared to L5, with a considerable proportion (25%, n = 197) of overactive neurons firing at > 5 Hz, for which the sensitivity in connection derivation was poorer than average too (13.8 ± 7.9%, Cohen's d = -2.99, $p < 0.05$). The main reason for the low sensitivity in the case of overactive neurons is a large proportion of false negatives that were estimated as non-connections due to peaks at lag 0 in the cross-correlograms, resulting from higher spike correlations between the overactive neurons than average (0.008 ± 0.008 vs 0.005 ± 0.008, Cohen's d = 0.4, $p < 0.05$). A reason for the lower PPV was that the increased firing of the overactive neurons resulted from recurrent activity, and thus followed underactive neurons,

leading to short-lag peaks in the cross-correlograms irrespective of connectivity and thus spurious connection derivation. In comparison, the remaining 58% (n = 456) of the neurons, which fired between 1 – 5 Hz, showed better connection derivation compared to average performance (sensitivity 69.9 ± 9.0%, Cohen's $d = 1.39$, $p < 0.05$).

We therefore tested another general activation paradigm that yielded a distribution of average L2/3 Pyr neuron spiking similar to L5 in addition to a similar mean Pyr firing rate of 3.4 ± 1.3 Hz. This paradigm involved a disinhibition of Pyr neurons by decreasing background input to PV and SST interneurons, together with a small decrease in Pyr background inputs. However, this activation by disinhibition led to more rhythmic and correlated firing than baseline (0.06 ± 0.02 vs 0.0008 ± 0.007, Cohen's $d = 3.65$, $p < 0.05$, Figure 2C), which resulted in increased spurious (false positive) derivation and thus poor PPV compared to baseline (29.1 ± 9.8%, Cohen's $d = -3.23$, $p < 0.05$, n = 800 neurons, Figure 2B). The disinhibition led to only a modest increase in sensitivity compared to baseline (34.3 ± 17.3%, Cohen's $d = 2.19$, $p < 0.05$, n = 800 neurons, Figure 2B) and thus was overall less successful than the general-Pyr activation paradigm.

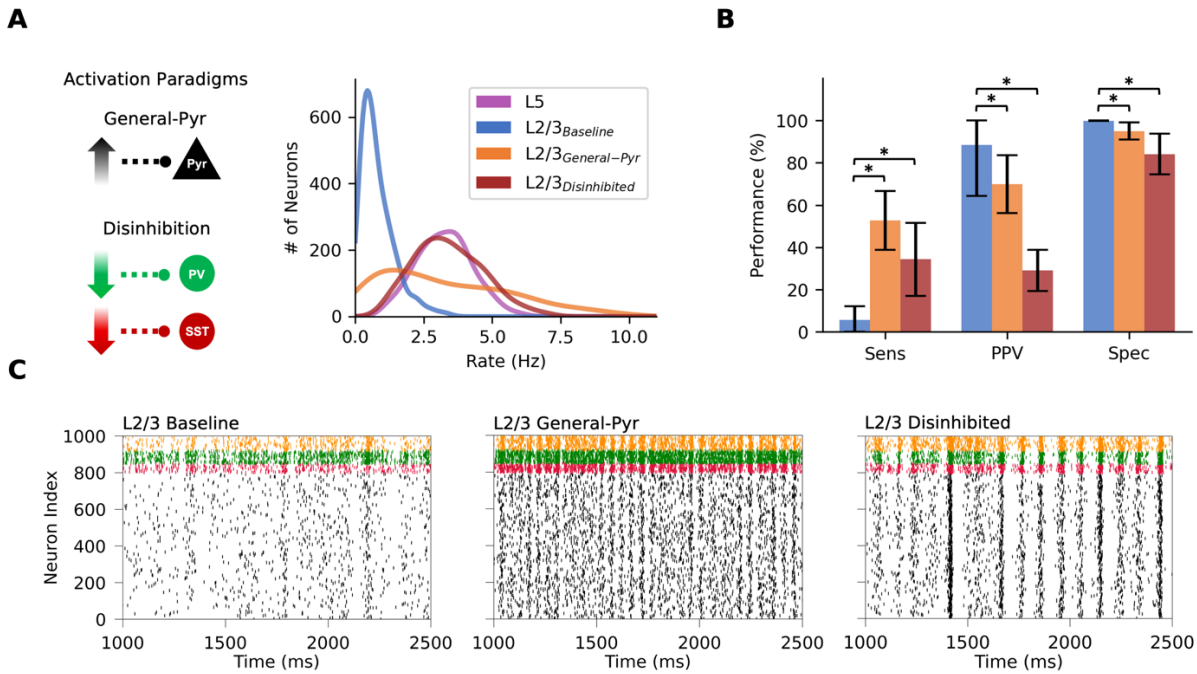

Figure 2. Moderate improvement in derivation of L2/3 connections by activation of Pyr neurons. (A) Left: The paradigms for activation of Pyr neurons in L2/3 microcircuits, either generally activating Pyr neurons or by disinhibition. Right: Distribution of average Pyr neuron spike rates in L5 baseline (purple, n = 700), L2/3 baseline (blue, n = 784), L2/3 general-Pyr (orange, n = 786), and L2/3 disinhibited (red, n = 800). Curves were smoothed using a Gaussian kernel. **(B)** Derivation performance (mean ± SD) for excitatory connections in L2/3 microcircuits at baseline, and in the general-Pyr and disinhibited paradigms (color-coded as in A). Asterisk denotes $p < 0.05$ and Cohen's $d > 0.5$. **(C)** Example raster plot of simulated spiking in L2/3 microcircuits at baseline (left), and in the general-Pyr (middle) and disinhibited (right) paradigms, color-coded according to neuron type.

We then tested a more refined activation paradigm, targeting a subset of 100 Pyr neurons and inducing moderate and jittered spiking (Figure 3A). This led to an increased mean firing rate (3.0 ± 1.1 Hz) only in the subset population and had little effect on the activity of the non-activated population (Figure 3B). The subset activation paradigm yielded a firing rate distribution similar to L5, with less inactive and overactive neuron populations compared to the same subset in the L2/3 general-Pyr paradigm (inactive portion = 3% vs 11%, overactive portion = 6% vs 20%, respectively, Figure 3C). Consequently, the subset activation paradigm improved the sensitivity of derivation performance compared to L2/3 general-Pyr (74.0 ± 15.2%, Cohen's d = 0.93, $p < 0.05$, Figure 3D) while maintaining a similarly fair PPV performance (73.4 ± 16.0%). A stronger subset activation (e.g. leading to 4.8 Hz) was less optimal due to poorer PPV (28.7 ± 8.3%).

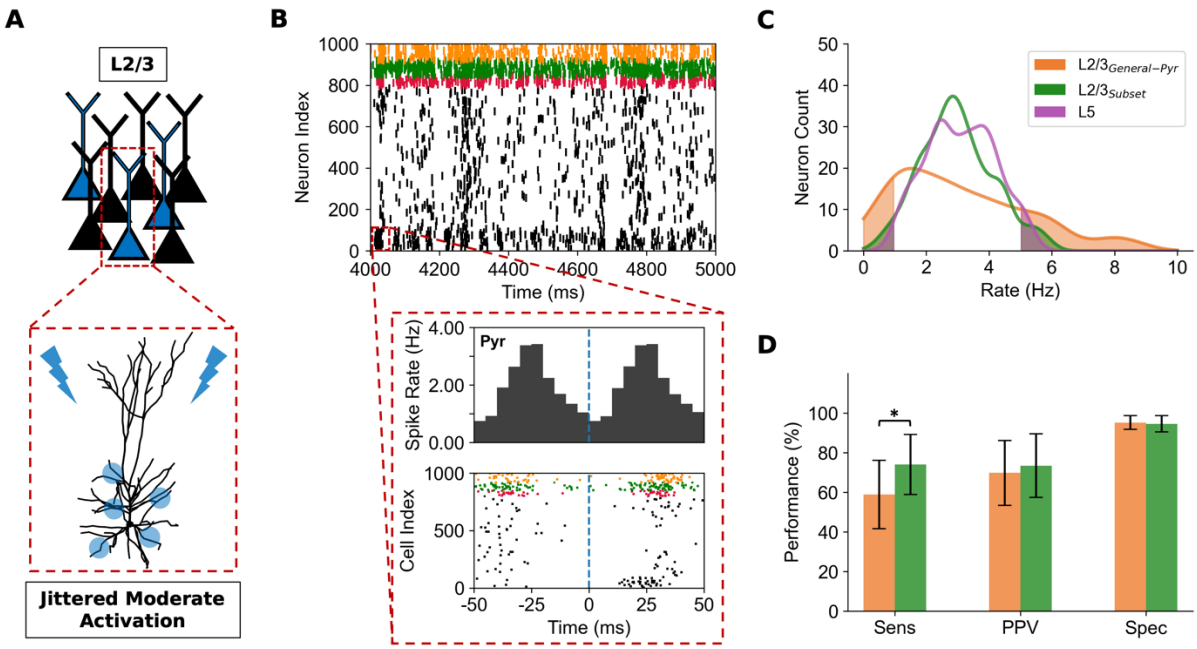

Figure 3. Improved true positive derivation of L2/3 connections by jittered moderate activation of Pyr neuron subset. (A) Schematic of simulation paradigm, where a subset of L2/3 Pyr neurons (blue) were activated repetitively by jittered moderate inputs (20 ms jitter, 50 ms cycles for 180 minutes). Inset: Schematic of synaptic contacts of the input along the basal dendrites. **(B)** Example raster plot of spiking in the L2/3 microcircuit during two cycles of the activated subset (first 100 neurons). Inset: peristimulus time histogram (top, n = 200 activation cycles) and example raster plot of spike response (bottom). A dashed line denotes stimulus onset. **(C)** Distribution of average Pyr neuron spike rates of the 100 L2/3 Pyr neuron subset (green) compared to in the L2/3 general-Pyr paradigm (orange) and a subset of 100 L5 Pyr neurons (black). The shaded regions represent the proportion of inactive (< 1 Hz) and overactive (> 5 Hz) neurons in each case. Curves were smoothed using a Gaussian kernel. **(D)** Derivation performance (mean ± SD) for excitatory connections for the 100 L2/3 Pyr neuron subset vs the general-Pyr paradigm (color-coded as in C). Asterisk denotes $p < 0.05$ and Cohen's $d > 0.5$.

We next compared derivation for connections from different inhibitory interneuron types onto Pyr neurons. PV→Pyr connections targeted proximal regions of the Pyr neuron (basal dendrites and soma) and could be derived using a short timescale like the Pyr→Pyr

connections (τ = 4 ms in both L5 and L2/3, Figure 4A). However, using the same parameters for SST→Pyr connections resulted in poor true positive derivation for both L5 (sensitivity = 43.4 ± 10.6%) and L2/3 (sensitivity = 2.9 ± 1.4%) microcircuits at baseline. Since SST interneurons targeted distal regions (apical dendrites), deriving their connections required using a longer decay time constant (τ = 8 ms and τ = 15 ms for SST→Pyr in L5 and L2/3, respectively, Figure 4B).

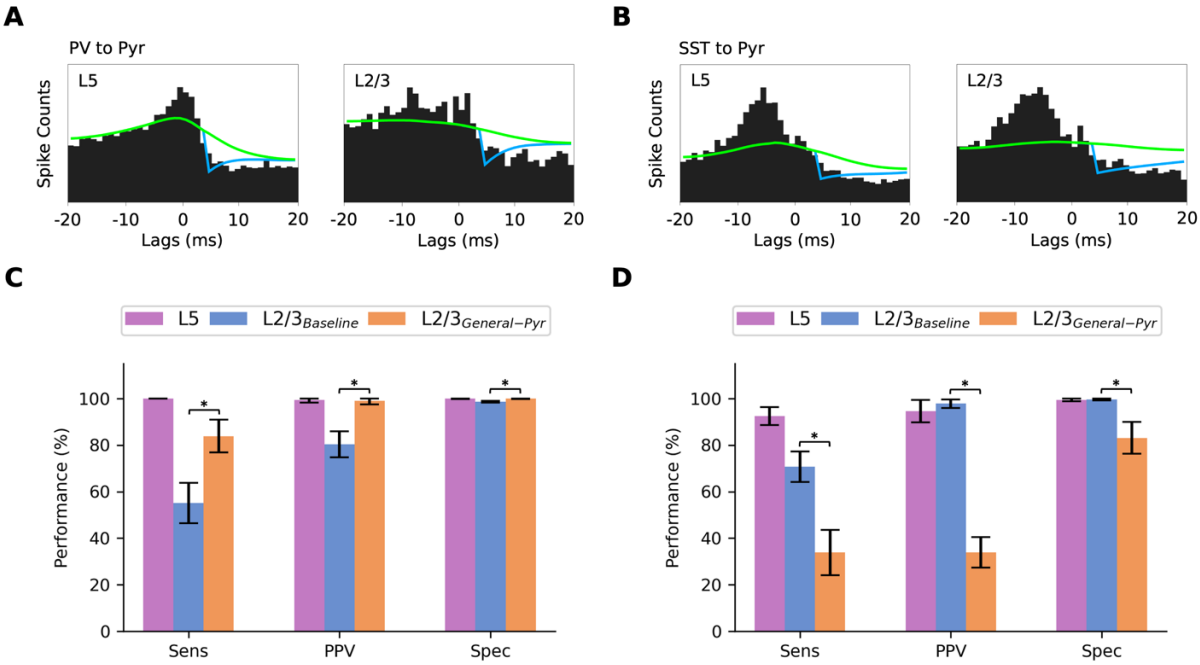

Figure 4. Connection derivation for PV vs SST inhibitory connections. (A) Cross-correlogram, derived connection (cyan) and slow fluctuation curve (green) for example derivations of true positive PV→Pyr connections in L5 (left) and L2/3 (right) microcircuits (τ = 4 ms for both). **(B)** Same as A, but for SST→Pyr connections (τ = 8 ms and τ = 15 ms in L5 and L2/3, respectively). **(C)** Derivation performance for PV→Pyr inhibitory connections in the different cases. **(D)** Same as C, but for SST→Pyr connections. Asterisk denotes $p < 0.05$ and Cohen's $d > 0.5$. Histograms in C and D show mean ± SD.

For the L5 microcircuit, inhibitory connections were derived with high accuracy for both PV→Pyr (sensitivity = 100.0 ± 0.0%; PPV = 99.4 ± 1.2%; n = 100 presynaptic neurons, Figure 4C) and SST→Pyr (sensitivity = 92.5 ± 3.9%; PPV = 94.7 ± 4.8%; n = 150 presynaptic neurons, Figure 4D). In the L2/3 microcircuit at baseline, however, derivation performance was lower for both PV→Pyr connections (sensitivity = 55.1 ± 8.6%; PPV = 80.4 ± 5.6%; n = 70 presynaptic neurons, Figure 4C) and SST→Pyr connections (sensitivity = 70.8 ± 6.5%; PPV = 97.8 ± 1.8%; n = 50 presynaptic neurons, Figure 4D), although better than for Pyr→Pyr connections. Derivation performance for these connections was averaged across presynaptic interneurons instead of postsynaptic pyramidal neurons to ensure adequate sample sizes. The low sensitivity in L2/3 at baseline was likely mostly due to the low firing rates in Pyr neurons,

as SST and PV interneurons fired at moderate rates (5.7 ± 0.9 Hz and 10.2 ± 2.9 Hz, respectively). The higher accuracy in SST→Pyr derivation compared to PV→Pyr in L2/3 baseline was likely due to the use of a longer decay time constant and thus larger information about the effects on postsynaptic neuron spiking in cross-correlations.

The L2/3 general-Pyr activation improved derivation performance in PV→Pyr connections (sensitivity = 83.9 ± 7.1%, Cohen's $d = 3.63$, $p < 0.05$; PPV = 99.1 ± 1.6%, Cohen's $d = 4.50$, $p < 0.05$, Figure 4C), due to increased postsynaptic Pyr firing rates. The sensitivity was still lower than in L5 derivation, likely due to issues with the inactive and overactive postsynaptic Pyr neurons described above for Pyr→Pyr connection derivation. Derivation performance for SST→Pyr connections decreased considerably in the L2/3 general-Pyr paradigm instead of improving (sensitivity = 33.9 ± 9.8%, Cohen's $d = -4.40$, $p < 0.05$; PPV = 33.9 ± 6.5%, Cohen's $d = -13.33$, $p < 0.05$, Figure 4D). This was due to the drastic increase in SST firing rates in the L2/3 general-Pyr paradigm (24.5 ± 5.4 Hz) and higher correlated firing of SST and Pyr neurons (SST-Pyr: 0.02 ± 0.009 vs 0.002 ± 0.007, Cohen's $d = 1.65$, $p < 0.05$; SST-SST: 0.06 ± 0.009 vs 0.009 ± 0.007, Cohen's $d = 5.48$, $p < 0.05$), leading to spurious connection derivation (false positives) and ignored connections (false negatives) due to lag 0 peaks in the cross-correlograms. The disinhibition paradigm resulted in even poorer derivation performance for both types of connections (PV→Pyr: sensitivity = 1.3 ± 1.3%, Cohen's $d = -8.70$, $p < 0.05$; SST→Pyr: sensitivity = 1.6 ± 1.0%, Cohen's $d = -14.71$, $p < 0.05$), due to even higher correlated firing in the microcircuit (SST-SST: 0.2 ± 0.01, Cohen's $d = 19.43$, $p < 0.05$; PV-PV: 0.2 ± 0.02 vs 0.01 ± 0.008, Cohen's $d = 13.23$, $p < 0.05$; SST-Pyr: 0.09 ± 0.02, Cohen's $d = 4.96$, $p < 0.05$; PV-Pyr: 0.1 ± 0.03 vs 0.003 ± 0.007, Cohen's $d = 4.70$, $p < 0.05$). Compared to L2/3 baseline and L2/3 general-Pyr, the subset activation paradigm led to further improvement of PV→Pyr connection derivation for the activated subset of Pyr neurons, yielding performance similar to L5 (sensitivity = 99.4 ± 2.5%, Cohen's $d = 3.35$, $p < 0.05$; PPV = 92.6 ± 10.0%, Cohen's $d = 1.00$, $p < 0.05$). On the other hand for SST→Pyr connections, whereas the subset activation similarly improved sensitivity (96.2 ± 5.1%, Cohen's $d = 2.47$, $p < 0.05$), PPV was poor as in general-Pyr activation (PPV = 35.0 ± 6.7%, Cohen's $d = -11.83$, $p < 0.05$).

Derivation performance for connections between different inhibitory interneurons was moderate for PV→SST and VIP→SST connections in the L5 microcircuit (sensitivity for PV→SST: 57.9 ± 16.5%; VIP→SST: 68.8 ± 15.0%) and in the L2/3 microcircuit at baseline

(sensitivity for PV→SST: 70.6 ± 33.1%; VIP→SST: 52.6 ± 12.6%), but poor for the rest of the connections between inhibitory interneurons. For similar reasons as described above, the L2/3 general-Pyr or disinhibition paradigms did not improve the performance for these connections either.

Discussion

In this work, we examined physiological challenges of deriving neuronal connectivity from baseline spiking activity, using detailed models of large-scale human cortical microcircuits in different layers. We showed that physiological properties of large-scale microcircuits had a significant impact on the performance of deriving Pyr neuron connections from spike cross-correlograms. We showed that silent and low-firing neurons in L2/3 led to poor derivation performance, and a general activation of the cortical microcircuit to increase firing rates yielded only a moderate improvement in connection derivation due to a trade-off between reducing inactive neurons and increasing correlated overactive neurons. We improved derivation using a more refined activation paradigm that induced moderate and jittered spiking with a reduced proportion of inactive and overactive neurons. In addition, we found that SST interneuron connections required a longer range of cross-correlation lags compared to PV interneurons, due to their distal synaptic contacts. Our results provide experimentally testable insights that can improve experimental derivation of neuronal connections from spiking activity, as recorded by dense multi-electrodes *in vivo* and at large scale.

The general microcircuit activation paradigms in the L2/3 microcircuit aimed to increase the average firing rate of Pyr neurons to resemble L5, which was active enough to yield good derivation. However, unlike the normal distribution of moderate firing rates in L5, the Pyr neurons in the L2/3 general-Pyr activation paradigm had populations of overactive and remaining underactive neurons hindering derivation performance. These results suggest that general activation, e.g. by pharmacology applied to the entire circuit[45], may have limited use with regards to connection derivation. The improvement we achieved using the more refined subset activation protocol for moderate jittered firing indicates the benefit of other paradigms such as a variety of sensory stimulus presentations e.g. using different orientations[44,46] or motion tasks[47,48] to activate subsets of neurons moderately and variably to further improve derivation performance. The subset activation was also able to improve derivation of PV→Pyr connections, but was less effective for deriving SST→Pyr connections, likely because the

activation involved basal stimulation of Pyr neurons, for which PV interneuron inhibition is more relevant.

Overcoming the challenge of microcircuit oscillations required shortening the cross-correlogram analysis window to less than the oscillation period, as it enabled the slow wave of the tool to better fit the baseline fluctuations near lag 0 and thus better detect connections on top of the baseline cross-correlation. Trying to improve PPV by excluding connections with peaks near lag 0 had a high cost on sensitivity, indicating that a sizeable proportion of neuron pairs that fired together were also connected, and thus the derivation would not benefit from excluding them. However, the tool's components were not sufficient to fit the overall shape of the cross-correlogram trough of inhibitory SST→Pyr connections which involved a slower rise time, resulting in moderate derivation performance and highlighting the tool's limitation of having only a single time constant parameter. Future studies should try to improve the tool by including both rise and decay time constants in the coupling filter.

Connection derivation in our microcircuit models required a slightly longer synaptic delay compared to previous studies[13,37]. A possible reason is that traditional parameters were based on rodent data, where neurons have shorter and less complex dendritic arbors than human neurons[49–51], and thus the delay between presynaptic spike and PSP at soma is shorter. While the cross-correlogram lag range used for connection derivation was comparable to previous studies, good derivation of L2/3 SST→Pyr connections necessitated a longer lag range compared to PV→Pyr connections due to the attenuation of SST IPSP from the distal apical synapses to the soma[52,53]. Deriving L5 SST→Pyr connections also required a long range but to a lesser extent, since human L5 Pyr neuron apical dendrites were less branched than those of L2/3 Pyr neurons in the reconstructed morphologies we used, and also on average as reported previously[43,44]. The proximal locations of PV→Pyr synapses resulted in stronger connections compared to SST→Pyr as seen experimentally[54,55], explaining the overall better derivation performance in L5, and a better improvement when activating L2/3. In this work we focused on connection detection rather than weight derivation, since the microcircuit models had the same conductance for all connections of a given type, with only the contact locations varying, resulting in a low range of synaptic weights. Future models should account for wider synaptic weight distributions as seen in the cortex[4] to study derivation performance in terms of connection weights.

Future works can refine our estimates of derivation performance by addressing issues that would arise from extracellular recordings such as noise[18,56] and spike sorting[57–59]. In addition, including a larger proportion of silent neurons as suggested experimentally[17,33–35] and

shared inputs among the neurons in the microcircuits[31,32] will help refine the estimated performance and the necessary activation paradigms. Future studies can also probe the effects of morphology[36] or physiological synaptic features such as multiple contacts, failure probability[60,61] and short-term dynamics on connection derivation.

Methods

Human cortical microcircuit models: We used detailed models of human cortical L5 microcircuits[44] and L2/3 microcircuits[43] as ground-truth data. Both microcircuit models consisted of 1000 detailed neuron models that reproduced firing rates, synaptic properties, and dendritic sag currents as measured in human neurons. The neurons were radially distributed in a volume with a 250 μm radius and a depth according to human cortical layer dimensions (L2/3 situated 250 μm – 1200 μm below the pia and L5 situated 1600 μm – 2300 μm below the pia)[62]. The models included key neuron types and proportions as measured in humans, and detailed reconstructed human morphologies; L5 circuit: 70% Pyr neurons, 15% SST, 10% PV, and 5% VIP interneurons[44]. L2/3 circuit: 80% Pyr, 5% SST, 7% PV, 8% VIP[43]. Pyr→Pyr connection probability was 0.15 in L2/3 and 0.09 in L5, as measured in humans[6,63], and other connection probabilities were as measured in rodents. PV interneurons targeted Pyr basal dendrites, while SST interneurons targeted Pyr apical dendrites. The neuron models included sodium, potassium, and calcium channels in the axon and soma, and h-current in the dendrites. For detailed descriptions of parameters such as synaptic conductance, all connection probabilities, and ion channel density values in L2/3 and L5, see Yao et al., 2022[43] and Guet-McCreight et al., 2023[44], respectively. The microcircuit models received random background excitatory inputs (neuron type specific) using Ornstein-Uhlenbeck (OU) point processes[64,65]. The models used AMPA and NMDA excitatory synapses ($\tau_{rise,NMDA}$ = 2 ms, $\tau_{decay,NMDA}$ = 65 ms, $\tau_{rise,AMPA}$ = 0.3 ms, $\tau_{decay,AMPA}$ = 3 ms), and $GABA_A$ inhibitory synapses ($\tau_{rise,GABA}$ = 1 ms, $\tau_{decay,GABA}$ = 10 ms). The synaptic reversal potentials were E_{exc} = 0 mV and E_{inh} = -80 mV. The models were simulated using NEURON[66], LFPy[67] and parallel computing in high-performance grid (SciNet)[68,69].

Neuronal connectivity derivation: We inferred putative monosynaptic connections by detecting short-lag peaks in cross-correlograms of simulated spike trains[13,37]. We used previous computational methods for fitting postsynaptic waveform curves to cross-correlograms[37] for improved derivation. We did a parameter search for the synaptic delay (d_s), interaction

timescale (τ), and flatness of slow fluctuation curve (γ) that yielded the best derivation performance. We tested synaptic delays ranging from d_s = 1 to 4 ms and slow fluctuation curves ranging from $\gamma = 2 \times 10^{-4}$ ms^{-1} (flatter) to 1×10^{-3} ms^{-1} (oscillatory). We determined the combination of d_s = 4 ms and $\gamma = 2 \times 10^{-4}$ ms^{-1} led to more balanced connection derivation performance. We used τ = 4 ms for all connection types except SST→Pyr (L5: τ = 8 ms, L2/3: τ = 15 ms), which required a longer τ due to the distal location of the synapses.

When deriving connections, we excluded silent neurons firing < 0.1 Hz as the lack of spike data incurred an error in the derivation tool and was not amenable to cross-correlation analysis. We evaluated derivation performance by calculating the sensitivity, PPV, and specificity.

General neuronal activation: We tested two general activation paradigms of L2/3 Pyr neurons to increase microcircuit activity, by changing background inputs to specific neuron types. L2/3 baseline excitatory OU conductance was: Pyr = 28 pS; SST = 30 pS; PV = 280 pS; VIP = 66 pS. In the L2/3 general-Pyr paradigm, background OU conductance in Pyr neurons was increased to 50 pS. In the L2/3 disinhibited paradigm, background OU conductance in SST and PV interneurons was reduced to 28 and 1 pS, respectively, and slightly reduced in Pyr neurons to 24 pS. Other disinhibition paradigms were less useful, e.g. reducing SST alone attenuated the overactive population at the expense of an increased proportion of low firing Pyr neuron population, and reducing PV alone led to a broad distribution with highly correlated firing. A combination of both was thus necessary to achieve the desired mean and distribution. In all microcircuit types and paradigms, the inhibitory component of the OU conductance was set to 0, as the recurrent inhibition in the microcircuit was sufficient to restrain excitability.

Subset neuronal activation: We activated a subset of 100 L2/3 Pyr neurons to induce moderate and jittered spiking, with firing rates similar to that of the L5 microcircuit while minimizing synchronous activity. Each Pyr neuron in the subset was activated using 5 excitatory AMPA/NMDA synapses, each with a conductance of 0.9 nS, distributed randomly on the basal dendrites. The repeated activations occurred in cycles of 50 ms, with jittered stimulus times (post-stimulus delay of 2 – 22 ms), repeating for 180 minutes.

Correlation tests: Discrete cross-correlations between neuron spike trains were calculated using normalized signals of spike time vectors using 300 seconds of spiking data, with spikes grouped into 3 ms bins. Before correlating, spike time vectors were normalized by subtracting

the mean from the signals and dividing by the product of the standard deviation and the vector length[70–72].

Statistical analysis: We determined statistical significance ($p < 0.05$) using paired and two-sample t-tests. We calculated the effect size between two conditions using Cohen's *d* (dividing the difference of two means by the overall standard deviation of all values).

Acknowledgements

We thank the Krembil Foundation for their generous funding support. FM was also supported by the Miner's Lamp Innovation Fund and by the Department of Physiology at the University of Toronto. MTH was also supported by NSERC and TCAIREM.

References

1. Gentet, L. J., Kremer, Y., Taniguchi, H., Huang, Z. J., Staiger, J. F., & Petersen, C. C. H. (2012). Unique functional properties of somatostatin-expressing GABAergic neurons in mouse barrel cortex. *Nature Neuroscience*, *15*(4), 607–612. https://doi.org/10.1038/nn.3051

2. Gal, E., London, M., Globerson, A., Ramaswamy, S., Reimann, M. W., Muller, E., Markram, H., & Segev, I. (2017). Rich cell-type-specific network topology in neocortical microcircuitry. *Nature Neuroscience*, *20*(7), 1004–1013. https://doi.org/10.1038/nn.4576

3. Yu, J., Hu, H., Agmon, A., & Svoboda, K. (2019). Recruitment of GABAergic Interneurons in the Barrel Cortex during Active Tactile Behavior. *Neuron*, *104*(2), 412-427.e4. https://doi.org/10.1016/j.neuron.2019.07.027

4. Song, S., Sjöström, P. J., Reigl, M., Nelson, S., & Chklovskii, D. B. (2005). Highly Nonrandom Features of Synaptic Connectivity in Local Cortical Circuits. *PLOS Biology*, *3*(3), e68. https://doi.org/10.1371/journal.pbio.0030068

5. Perin, R., Berger, T. K., & Markram, H. (2011). A synaptic organizing principle for cortical neuronal groups. *Proceedings of the National Academy of Sciences*, *108*(13), 5419–5424. https://doi.org/10.1073/pnas.1016051108

6. Campagnola, L., Seeman, S. C., Chartrand, T., Kim, L., Hoggarth, A., Gamlin, C., Ito, S., Trinh, J., Davoudian, P., Radaelli, C., Kim, M.-H., Hage, T., Braun, T., Alfiler, L., Andrade, J., Bohn, P., Dalley, R., Henry, A., Kebede, S., … Jarsky, T. (2022). Local connectivity and synaptic dynamics in mouse and human neocortex. *Science*, *375*(6585), eabj5861. https://doi.org/10.1126/science.abj5861

7. Sharf, T., van der Molen, T., Glasauer, S. M. K., Guzman, E., Buccino, A. P., Luna, G., Cheng, Z., Audouard, M., Ranasinghe, K. G., Kudo, K., Nagarajan, S. S., Tovar, K. R., Petzold, L. R., Hierlemann, A., Hansma, P. K., & Kosik, K. S. (2022). Functional neuronal circuitry and oscillatory dynamics in human brain organoids. *Nature Communications*, *13*(1), 4403. https://doi.org/10.1038/s41467-022-32115-4

8. Seney, M. L., Tripp, A., McCune, S., A. Lewis, D., & Sibille, E. (2015). Laminar and cellular analyses of reduced somatostatin gene expression in the subgenual anterior cingulate cortex in major depression. *Neurobiology of Disease*, *73*, 213–219. https://doi.org/10.1016/j.nbd.2014.10.005

9. Duman, R. S., Sanacora, G., & Krystal, J. H. (2019). Altered Connectivity in Depression: GABA and Glutamate Neurotransmitter Deficits and Reversal by Novel Treatments. *Neuron*, *102*(1), 75–90. https://doi.org/10.1016/j.neuron.2019.03.013

10. Lazarus, M. S., Krishnan, K., & Huang, Z. J. (2015). GAD67 Deficiency in Parvalbumin Interneurons Produces Deficits in Inhibitory Transmission and Network Disinhibition in Mouse Prefrontal Cortex. *Cerebral Cortex (New York, NY)*, *25*(5), 1290–1296. https://doi.org/10.1093/cercor/bht322

11. Toker, L., Mancarci, B. O., Tripathy, S., & Pavlidis, P. (2018). Transcriptomic Evidence for Alterations in Astrocytes and Parvalbumin Interneurons in Subjects With Bipolar Disorder and Schizophrenia. *Biological Psychiatry*, *84*(11), 787–796. https://doi.org/10.1016/j.biopsych.2018.07.010

12. Barthó, P., Hirase, H., Monconduit, L., Zugaro, M., Harris, K. D., & Buzsáki, G. (2004). Characterization of Neocortical Principal Cells and Interneurons by Network Interactions and Extracellular Features. *Journal of Neurophysiology*, *92*(1), 600–608. https://doi.org/10.1152/jn.01170.2003

13. Peyrache, A., Dehghani, N., Eskandar, E. N., Madsen, J. R., Anderson, W. S., Donoghue, J. A., Hochberg, L. R., Halgren, E., Cash, S. S., & Destexhe, A. (2012). Spatiotemporal dynamics of neocortical excitation and inhibition during human sleep. *Proceedings of the National Academy of Sciences*, *109*(5), 1731–1736. https://doi.org/10.1073/pnas.1109895109

14. Vizuete, J. A., Pillay, S., Diba, K., Ropella, K. M., & Hudetz, A. G. (2012). Monosynaptic functional connectivity in cerebral cortex during wakefulness and under graded levels of anesthesia. *Frontiers in Integrative Neuroscience*, *6*, 90. https://doi.org/10.3389/fnint.2012.00090

15. Jun, J. J., Steinmetz, N. A., Siegle, J. H., Denman, D. J., Bauza, M., Barbarits, B., Lee, A. K., Anastassiou, C. A., Andrei, A., Aydın, Ç., Barbic, M., Blanche, T. J., Bonin, V., Couto, J., Dutta, B., Gratiy, S. L., Gutnisky, D. A., Häusser, M., Karsh, B., … Harris, T. D. (2017). Fully integrated silicon probes for high-density recording of neural activity. *Nature*, *551*(7679), 232–236. https://doi.org/10.1038/nature24636

16. Steinmetz, N. A., Aydin, C., Lebedeva, A., Okun, M., Pachitariu, M., Bauza, M., Beau, M., Bhagat, J., Böhm, C., Broux, M., Chen, S., Colonell, J., Gardner, R. J., Karsh, B., Kloosterman, F., Kostadinov, D., Mora-Lopez, C., O'Callaghan, J., Park, J., … Harris, T. D. (2021). Neuropixels 2.0: A miniaturized high-density probe for stable, long-term

brain recordings. *Science*, *372*(6539), eabf4588. https://doi.org/10.1126/science.abf4588

17. Shoham, S., O'Connor, D. H., & Segev, R. (2006). How silent is the brain: Is there a "dark matter" problem in neuroscience? *Journal of Comparative Physiology A*, *192*(8), 777–784. https://doi.org/10.1007/s00359-006-0117-6

18. Buzsáki, G., & Draguhn, A. (2004). Neuronal Oscillations in Cortical Networks. *Science*, *304*(5679), 1926–1929. https://doi.org/10.1126/science.1099745

19. Noguchi, A., Ikegaya, Y., & Matsumoto, N. (2021). In Vivo Whole-Cell Patch-Clamp Methods: Recent Technical Progress and Future Perspectives. *Sensors (Basel, Switzerland)*, *21*(4), 1448. https://doi.org/10.3390/s21041448

20. Peng, Y., Mittermaier, F. X., Planert, H., Schneider, U. C., Alle, H., & Geiger, J. R. P. (2019). High-throughput microcircuit analysis of individual human brains through next-generation multineuron patch-clamp. *eLife*, *8*, e48178. https://doi.org/10.7554/eLife.48178

21. Kubota, Y., Sohn, J., & Kawaguchi, Y. (2018). Large Volume Electron Microscopy and Neural Microcircuit Analysis. *Frontiers in Neural Circuits*, *12*. https://www.frontiersin.org/articles/10.3389/fncir.2018.00098

22. Peddie, C. J., Genoud, C., Kreshuk, A., Meechan, K., Micheva, K. D., Narayan, K., Pape, C., Parton, R. G., Schieber, N. L., Schwab, Y., Titze, B., Verkade, P., Weigel, A., & Collinson, L. M. (2022). Volume electron microscopy. *Nature Reviews Methods Primers*, *2*(1), Article 1. https://doi.org/10.1038/s43586-022-00131-9

23. Hayworth, K. J., Xu, C. S., Lu, Z., Knott, G. W., Fetter, R. D., Tapia, J. C., Lichtman, J. W., & Hess, H. F. (2015). Ultrastructurally smooth thick partitioning and volume stitching for large-scale connectomics. *Nature Methods*, *12*(4), 319–322. https://doi.org/10.1038/nmeth.3292

24. Zheng, Z., Lauritzen, J. S., Perlman, E., Robinson, C. G., Nichols, M., Milkie, D., Torrens, O., Price, J., Fisher, C. B., Sharifi, N., Calle-Schuler, S. A., Kmecova, L., Ali, I. J., Karsh, B., Trautman, E. T., Bogovic, J. A., Hanslovsky, P., Jefferis, G. S. X. E., Kazhdan, M., … Bock, D. D. (2018). A Complete Electron Microscopy Volume of the Brain of Adult Drosophila melanogaster. *Cell*, *174*(3), 730-743.e22. https://doi.org/10.1016/j.cell.2018.06.019

25. Shapson-Coe, A., Januszewski, M., Berger, D. R., Pope, A., Wu, Y., Blakely, T., Schalek, R. L., Li, P. H., Wang, S., Maitin-Shepard, J., Karlupia, N., Dorkenwald, S., Sjostedt, E., Leavitt, L., Lee, D., Troidl, J., Collman, F., Bailey, L., Fitzmaurice, A., … Lichtman, J. W. (2024). A petavoxel fragment of human cerebral cortex reconstructed at nanoscale resolution. *Science*, *384*(6696), eadk4858. https://doi.org/10.1126/science.adk4858

26. Schneider-Mizell, C. M., Gerhard, S., Longair, M., Kazimiers, T., Li, F., Zwart, M. F., Champion, A., Midgley, F. M., Fetter, R. D., Saalfeld, S., & Cardona, A. (2016). Quantitative neuroanatomy for connectomics in Drosophila. *eLife*, *5*, e12059. https://doi.org/10.7554/eLife.12059

27. Dorkenwald, S., Schubert, P. J., Killinger, M. F., Urban, G., Mikula, S., Svara, F., & Kornfeld, J. (2017). Automated synaptic connectivity inference for volume electron microscopy. *Nature Methods*, *14*(4), Article 4. https://doi.org/10.1038/nmeth.4206

28. Fujisawa, S., Amarasingham, A., Harrison, M. T., & Buzsáki, G. (2008). Behavior-dependent short-term assembly dynamics in the medial prefrontal cortex. *Nature Neuroscience*, *11*(7), 823–833. https://doi.org/10.1038/nn.2134

29. De Blasi, S., Ciba, M., Bahmer, A., & Thielemann, C. (2019). Total spiking probability edges: A cross-correlation based method for effective connectivity estimation of cortical spiking neurons. *Journal of Neuroscience Methods*, *312*, 169–181. https://doi.org/10.1016/j.jneumeth.2018.11.013

30. Siegle, J. H., Jia, X., Durand, S., Gale, S., Bennett, C., Graddis, N., Heller, G., Ramirez, T. K., Choi, H., Luviano, J. A., Groblewski, P. A., Ahmed, R., Arkhipov, A., Bernard, A., Billeh, Y. N., Brown, D., Buice, M. A., Cain, N., Caldejon, S., … Koch, C. (2021). Survey of spiking in the mouse visual system reveals functional hierarchy. *Nature*, *592*(7852), 86–92. https://doi.org/10.1038/s41586-020-03171-x

31. Ecker, A. S., Berens, P., Keliris, G. A., Bethge, M., Logothetis, N. K., & Tolias, A. S. (2010). Decorrelated Neuronal Firing in Cortical Microcircuits. *Science*, *327*(5965), 584–587.

32. Renart, A., de la Rocha, J., Bartho, P., Hollender, L., Parga, N., Reyes, A., & Harris, K. D. (2010). The Asynchronous State in Cortical Circuits. *Science*, *327*(5965), 587–590.

33. Gur, M., Kagan, I., & Snodderly, D. M. (2005). Orientation and Direction Selectivity of Neurons in V1 of Alert Monkeys: Functional Relationships and Laminar Distributions. *Cerebral Cortex*, *15*(8), 1207–1221. https://doi.org/10.1093/cercor/bhi003

34. Gur, M., & Snodderly, D. M. (2008). Physiological differences between neurons in layer 2 and layer 3 of primary visual cortex (V1) of alert macaque monkeys. *The Journal of Physiology*, *586*(9), 2293–2306. https://doi.org/10.1113/jphysiol.2008.151795

35. O'Connor, D. H., Peron, S. P., Huber, D., & Svoboda, K. (2010). Neural Activity in Barrel Cortex Underlying Vibrissa-Based Object Localization in Mice. *Neuron*, *67*(6), 1048–1061. https://doi.org/10.1016/j.neuron.2010.08.026

36. Beniaguev, D., Segev, I., & London, M. (2021). Single cortical neurons as deep artificial neural networks. *Neuron*, *109*(17), 2727-2739.e3. https://doi.org/10.1016/j.neuron.2021.07.002

37. Kobayashi, R., Kurita, S., Kurth, A., Kitano, K., Mizuseki, K., Diesmann, M., Richmond, B. J., & Shinomoto, S. (2019). Reconstructing neuronal circuitry from parallel spike trains. *Nature Communications*, *10*(1), 4468. https://doi.org/10.1038/s41467-019-12225-2

38. Endo, D., Kobayashi, R., Bartolo, R., Averbeck, B. B., Sugase-Miyamoto, Y., Hayashi, K., Kawano, K., Richmond, B. J., & Shinomoto, S. (2021). A convolutional neural network for estimating synaptic connectivity from spike trains. *Scientific Reports*, *11*(1), 12087. https://doi.org/10.1038/s41598-021-91244-w

39. Vareberg, A. D., Bok, I., Eizadi, J., Ren, X., & Hai, A. (2024). Inference of network connectivity from temporally binned spike trains. *Journal of Neuroscience Methods*, *404*, 110073. https://doi.org/10.1016/j.jneumeth.2024.110073

40. Ren, X., Bok, I., Vareberg, A., & Hai, A. (2023). Stimulation-mediated reverse engineering of silent neural networks. *Journal of Neurophysiology*, *129*(6), 1505–1514. https://doi.org/10.1152/jn.00100.2023

41. Vidne, M., Ahmadian, Y., Shlens, J., Pillow, J. W., Kulkarni, J., Litke, A. M., Chichilnisky, E. J., Simoncelli, E., & Paninski, L. (2012). Modeling the impact of common noise inputs on the network activity of retinal ganglion cells. *Journal of Computational Neuroscience*, *33*(1), 97–121. https://doi.org/10.1007/s10827-011-0376-2

42. Soudry, D., Keshri, S., Stinson, P., Oh, M., Iyengar, G., & Paninski, L. (2015). Efficient 'Shotgun' Inference of Neural Connectivity from Highly Sub-sampled Activity Data. *PLOS Computational Biology*, *11*(10), e1004464. https://doi.org/10.1371/journal.pcbi.1004464

43. Yao, H. K., Guet-McCreight, A., Mazza, F., Chameh, H. M., Prevot, T. D., Griffiths, J. D., Tripathy, S. J., Valiante, T. A., Sibille, E., & Hay, E. (2022). Reduced inhibition in depression impairs stimulus processing in human cortical microcircuits. *Cell Reports*, *38*(2). https://doi.org/10.1016/j.celrep.2021.110232

44. Guet-McCreight, A., Chameh, H. M., Mahallati, S., Wishart, M., Tripathy, S. J., Valiante, T. A., & Hay, E. (2023). Age-dependent increased sag amplitude in human pyramidal neurons dampens baseline cortical activity. *Cerebral Cortex*, *33*(8), 4360–4373. https://doi.org/10.1093/cercor/bhac348

45. Florez, C. M., McGinn, R. J., Lukankin, V., Marwa, I., Sugumar, S., Dian, J., Hazrati, L.-N., Carlen, P. L., Zhang, L., & Valiante, T. A. (2015). In Vitro Recordings of Human Neocortical Oscillations. *Cerebral Cortex*, *25*(3), 578–597. https://doi.org/10.1093/cercor/bht235

46. Song, W., & Semework, M. (2015). Tactile representation in somatosensory thalamus (VPL) and cortex (S1) of awake primate and the plasticity induced by VPL neuroprosthetic stimulation. *Brain Research*, *1625*, 301–313. https://doi.org/10.1016/j.brainres.2015.08.046

47. Thompson, L. W., Kim, B., Rokers, B., & Rosenberg, A. (2023). Hierarchical computation of 3D motion across macaque areas MT and FST. *Cell Reports*, *42*(12). https://doi.org/10.1016/j.celrep.2023.113524

48. Doudlah, R., Chang, T.-Y., Thompson, L. W., Kim, B., Sunkara, A., & Rosenberg, A. (2022). Parallel processing, hierarchical transformations, and sensorimotor associations along the 'where' pathway. *eLife*, *11*, e78712. https://doi.org/10.7554/eLife.78712

49. Mihaljević, B., Larrañaga, P., Benavides-Piccione, R., DeFelipe, J., & Bielza, C. (2020). Comparing basal dendrite branches in human and mouse hippocampal CA1 pyramidal neurons with Bayesian networks. *Scientific Reports*, *10*(1), 18592. https://doi.org/10.1038/s41598-020-73617-9

50. Kalmbach, B. E., Hodge, R. D., Jorstad, N. L., Owen, S., Frates, R. de, Yanny, A. M., Dalley, R., Mallory, M., Graybuck, L. T., Radaelli, C., Keene, C. D., Gwinn, R. P., Silbergeld, D. L., Cobbs, C., Ojemann, J. G., Ko, A. L., Patel, A. P., Ellenbogen, R. G., Bakken, T. E., … Ting, J. T. (2021). Signature morpho-electric, transcriptomic, and dendritic properties of human layer 5 neocortical pyramidal neurons. *Neuron*, *109*(18), 2914-2927.e5. https://doi.org/10.1016/j.neuron.2021.08.030

51. Moradi Chameh, H., Rich, S., Wang, L., Chen, F.-D., Zhang, L., Carlen, P. L., Tripathy, S. J., & Valiante, T. A. (2021). Diversity amongst human cortical pyramidal neurons revealed via their sag currents and frequency preferences. *Nature Communications*, *12*(1), 2497. https://doi.org/10.1038/s41467-021-22741-9

52. Kole, M. H. P., Letzkus, J. J., & Stuart, G. J. (2007). Axon Initial Segment Kv1 Channels Control Axonal Action Potential Waveform and Synaptic Efficacy. *Neuron*, *55*(4), 633–647. https://doi.org/10.1016/j.neuron.2007.07.031

53. Alberts, B., Johnson, A., Lewis, J., Raff, M., Roberts, K., & Walter, P. (2002). Ion Channels and the Electrical Properties of Membranes. In *Molecular Biology of the Cell. 4th edition*. Garland Science. https://www.ncbi.nlm.nih.gov/books/NBK26910/

54. Dorsett, C., Philpot, B. D., Smith, S. L., & Smith, I. T. (2021). The Impact of SST and PV Interneurons on Nonlinear Synaptic Integration in the Neocortex. *eNeuro*, *8*(5). https://doi.org/10.1523/ENEURO.0235-21.2021

55. Fernandez, F. R., Via, G., Canavier, C. C., & White, J. A. (2022). Kinetics and Connectivity Properties of Parvalbumin- and Somatostatin-Positive Inhibition in Layer 2/3 Medial Entorhinal Cortex. *eNeuro*, *9*(1). https://doi.org/10.1523/ENEURO.0441-21.2022

56. Henze, D. A., Borhegyi, Z., Csicsvari, J., Mamiya, A., Harris, K. D., & Buzsáki, G. (2000). Intracellular Features Predicted by Extracellular Recordings in the Hippocampus In Vivo. *Journal of Neurophysiology*, *84*(1), 390–400. https://doi.org/10.1152/jn.2000.84.1.390

57. Pillow, J. W., Shlens, J., Paninski, L., Sher, A., Litke, A. M., Chichilnisky, E. J., & Simoncelli, E. P. (2008). Spatio-temporal correlations and visual signalling in a complete neuronal population. *Nature*, *454*(7207), Article 7207. https://doi.org/10.1038/nature07140

58. Pachitariu, M., Sridhar, S., Pennington, J., & Stringer, C. (2024). Spike sorting with Kilosort4. *Nature Methods*, *21*(5), 914–921. https://doi.org/10.1038/s41592-024-02232-7

59. Mizuseki, K., Sirota, A., Pastalkova, E., & Buzsáki, G. (2009). Theta Oscillations Provide Temporal Windows for Local Circuit Computation in the Entorhinal-Hippocampal Loop. *Neuron*, *64*(2), 267–280. https://doi.org/10.1016/j.neuron.2009.08.037

60. Ramaswamy, S., Courcol, J.-D., Abdellah, M., Adaszewski, S. R., Antille, N., Arsever, S., Atenekeng, G., Bilgili, A., Brukau, Y., Chalimourda, A., Chindemi, G., Delalondre, F., Dumusc, R., Eilemann, S., Gevaert, M. E., Gleeson, P., Graham, J. W., Hernando, J. B., Kanari, L., … Markram, H. (2015). The neocortical microcircuit collaboration portal:

A resource for rat somatosensory cortex. *Frontiers in Neural Circuits*, *9*. https://doi.org/10.3389/fncir.2015.00044

61. Markram, H., Muller, E., Ramaswamy, S., Reimann, M. W., Abdellah, M., Sanchez, C. A., Ailamaki, A., Alonso-Nanclares, L., Antille, N., Arsever, S., Kahou, G. A. A., Berger, T. K., Bilgili, A., Buncic, N., Chalimourda, A., Chindemi, G., Courcol, J.-D., Delalondre, F., Delattre, V., … Schürmann, F. (2015). Reconstruction and Simulation of Neocortical Microcircuitry. *Cell*, *163*(2), 456–492. https://doi.org/10.1016/j.cell.2015.09.029

62. Mohan, H., Verhoog, M. B., Doreswamy, K. K., Eyal, G., Aardse, R., Lodder, B. N., Goriounova, N. A., Asamoah, B., B. Brakspear, A. B. C., Groot, C., van der Sluis, S., Testa-Silva, G., Obermayer, J., Boudewijns, Z. S. R. M., Narayanan, R. T., Baayen, J. C., Segev, I., Mansvelder, H. D., & de Kock, C. P. J. (2015). Dendritic and Axonal Architecture of Individual Pyramidal Neurons across Layers of Adult Human Neocortex. *Cerebral Cortex*, *25*(12), 4839–4853. https://doi.org/10.1093/cercor/bhv188

63. Seeman, S. C., Campagnola, L., Davoudian, P. A., Hoggarth, A., Hage, T. A., Bosma-Moody, A., Baker, C. A., Lee, J. H., Mihalas, S., Teeter, C., Ko, A. L., Ojemann, J. G., Gwinn, R. P., Silbergeld, D. L., Cobbs, C., Phillips, J., Lein, E., Murphy, G., Koch, C., … Jarsky, T. (2018). Sparse recurrent excitatory connectivity in the microcircuit of the adult mouse and human cortex. *eLife*, *7*, e37349. https://doi.org/10.7554/eLife.37349

64. Fellous, J.-M., Rudolph, M., Destexhe, A., & Sejnowski, T. J. (2003). Synaptic background noise controls the input/output characteristics of single cells in an in vitro model of in vivo activity. *Neuroscience*, *122*(3), 811–829. https://doi.org/10.1016/j.neuroscience.2003.08.027

65. Destexhe, A., Rudolph, M., Fellous, J.-M., & Sejnowski, T. J. (2001). Fluctuating synaptic conductances recreate in vivo-like activity in neocortical neurons. *Neuroscience*, *107*(1), 13–24. https://doi.org/10.1016/S0306-4522(01)00344-X

66. Carnevale, N. T., & Hines, M. L. (2006). *The NEURON Book*. Cambridge University Press. https://doi.org/10.1017/CBO9780511541612

67. Hagen, E., Næss, S., Ness, T. V., & Einevoll, G. T. (2018). Multimodal Modeling of Neural Network Activity: Computing LFP, ECoG, EEG, and MEG Signals With LFPy 2.0. *Frontiers in Neuroinformatics*, *12*. https://doi.org/10.3389/fninf.2018.00092

68. Loken, C., Gruner, D., Groer, L., Peltier, R., Bunn, N., Craig, M., Henriques, T., Dempsey, J., Yu, C.-H., Chen, J., Dursi, L. J., Chong, J., Northrup, S., Pinto, J., Knecht, N., & Zon, R. V. (2010). SciNet: Lessons Learned from Building a Power-efficient Top-20 System and Data Centre. *Journal of Physics: Conference Series*, *256*(1), 012026. https://doi.org/10.1088/1742-6596/256/1/012026

69. Ponce, M., van Zon, R., Northrup, S., Gruner, D., Chen, J., Ertinaz, F., Fedoseev, A., Groer, L., Mao, F., Mundim, B. C., Nolta, M., Pinto, J., Saldarriaga, M., Slavnic, V., Spence, E., Yu, C.-H., & Peltier, W. R. (2019). Deploying a Top-100 Supercomputer for Large Parallel Workloads: The Niagara Supercomputer. *Practice and Experience in Advanced*

Research Computing 2019: Rise of the Machines (Learning). https://doi.org/10.1145/3332186.3332195

70. Howell, D. C. (2013). *Statistical methods for psychology* (8th ed.). Wadsworth Cengage Learning.

71. Jain, A., Nandakumar, K., & Ross, A. (2005). Score normalization in multimodal biometric systems. *Pattern Recognition*, *38*(12), 2270–2285. https://doi.org/10.1016/j.patcog.2005.01.012

72. Guan, Z., & Wang, Y. (2023). Data-driven simulation of two-dimensional cross-correlated random fields from limited measurements using joint sparse representation. *Reliability Engineering & System Safety*, *238*, 109408. https://doi.org/10.1016/j.ress.2023.109408